Shape controllable synthesis and enhanced upconversion photoluminescence of β-$NaGdF_4$:Yb^{3+}, Er^{3+} nanocrystals by introducing Mg^{2+}*

Yong-Xin Yang(杨永馨)[1,2], Zheng Xu(徐征)[1,2,†], Su-Ling Zhao(赵谡玲)[1,2], Zhi-Qin Liang(梁志琴)[1,2], Wei Zhu(朱薇)[1,2], and Jun-Jie Zhang(张俊杰)[1,2]

[1] *Key Laboratory of Luminescence and Optical Information, Ministry of Education, Beijing Jiaotong University, Beijing* 100044, *China*
[2] *Institute of Optoelectronics Technology, Beijing Jiaotong University, Beijing* 100044, *China*

(Received 16 February 2017; revised manuscript received 8 May 2017; published online 20 June 2017)

Different concentrations of Mg^{2+}-doped hexagonal phase $NaGdF_4$:Yb^{3+}, Er^{3+} nanocrystals (NCs) were synthesized by a modified solvothermal method. Successful codoping of Mg^{2+} ions in upconversion nanoparticles (UCNPs) was supported by XRD, SEM, EDS, and PL analyses. The effects of Mg^{2+} doping on the morphology and the intensity of the upconversion (UC) emission were discussed in detail. It turned out that with the concentration of Mg^{2+} increasing, the morphology of the nanoparticles turn to change gradually and the UC emission was increasing gradually as well. Notably the UC fluorescence intensities of Er^{3+} were gradually improved owing to the codoped Mg^{2+} and then achieved a maximum level as the concentration of Mg^{2+} ions was 60 mol% from the amendment of the crystal structure of β-$NaGdF_4$:Yb^{3+}, Er^{3+} nanoparticles. Moreover, the UC luminescence properties of the rare-earth (Yb^{3+}, Er^{3+}) ions codoped $NaGdF_4$ nanocrystals were investigated in detail under 980-nm excitation.

Keywords: $NaGdF_4$:Yb^{3+}/Er^{3+} nanoparticles, Mg^{2+}ions, morphology, upconversion photoluminescence

PACS: 78.40.–q, 74.25.Gz, 42.70.–a, 78.67.Bf **DOI:** 10.1088/1674-1056/26/8/087801

1. Introduction

Lanthanide-doped nanocrystals are the new-fashioned genre of nanomaterials which exhibit diverting luminescent and magnetic properties.[1–4] The distinct luminescent properties urged the conversion of low-energy photons to high-energy photons by multiphoton routes. The host materials $NaGdF_4$ already had a wide range of applications in biomedical fields among various forms of lanthanide-doped nanoparticles,[5,6] due to their multicolour emission character by doping rare earth ions and multifunction for surface functionalization. For instance, they played a perfect role that enabled them to significantly improve the quality of luminescence biomedical imaging,[7–9] multiplexed biological labeling and therapy.[10–14] Meanwhile, due to the feature that the NIR part of the solar spectrum could be converted to be visible in solar cells,[15,16] $NaGdF_4$ are also regarded as a potential candidate for improving solar energy utilization. As they mainly depended on electronic transition probabilities, upconversion luminescence intensities of rare earth ions enable them to be destroyed by the local crystal field of the rare-earth ions. So the effective strategies to increase the upconversion emissions appeared accordingly as follows, first of all, the probability of an extremely efficient resonant or near-resonant process should be increased,[17,18] and meanwhile the crystal symmetry should be reduced via tailing the local crystal field of the rare-earth ions.[19,20] Recently, Dong *et al.* successfully fabricated luminescent–magnetic bifunctional $NaGdF_4$:Dy^{3+}, Eu^{3+} nanomaterials and achieved the tunable multicolor luminescence,[21] while Parthiban Ramasamy *et al.* synthesized $NaGdF_4$:Yb^{3+}, Er^{3+} nanocrystals by Fe^{3+} doping with the enhanced upconversion luminescence and discussed their application in bioimaging.[22] At the same time, Lei *et al.* introduced Ca^{2+} dopants into the grain lattices by substituting Gd^{3+} ions, then the irregular $NaGdF_4$:Yb^{3+}, Er^{3+} nanocrystals converted into highly uniform nanorods. Meanwhile, they acquired highly intensified upconversion luminescence due to an amendment of the crystal structure of $NaGdF_4$.[23]

In our study, a new strategy to enhance upconversion emission has been realized based on β-$NaGdF_4$:Yb^{3+}, Er^{3+} nanocrystals tridoping with Mg^{2+} ions which had a series of high concentrations for the first time. Notably, the results demonstrate that via Mg^{2+} doping in the system, F^- vacancies formed, which results in a conversion of the morphology of Mg^{2+}-doped $NaGdF_4$:Yb^{3+}, Er^{3+} NCs from shaped nanoparticles to hexagonal nanoplates. Moreover, it has turned out that with the concentration of Mg^{2+} increasing, not only the intensity of green UC emission but also the intensity of red

*Project supported by the National High Technology Research and Development Program of China (Grant No. 2013AA032205), the Key Project of Beijing Scientific Committee, China (Grant No. D161100003416001), the Fundamental Research Funds for the Central Universities, China (Grant No. 2016JBM066), and the National Natural Science Foundation of China (Grant Nos. 51272022 and 11474018).

†Corresponding author. E-mail: zhengxu@bjtu.edu.cn

© 2017 Chinese Physical Society and IOP Publishing Ltd

UC emission increase at the same time. It is worth noting that the growth of red UC emission is more outstanding, which is conducive to the detection of biological utilizing visible red emission.

2. Experimental section

2.1. Synthesis of hexagonal phase $NaGdF_4$:Yb^{3+}, Er^{3+} nanocrystals

$\beta-NaGdF_4$ UCNPs codoped with 20-mol% Yb^{3+}, 2-mol% Er^{3+} and 0-, 40-, 50-, 60-, and 70-mol% Mg^{2+} ions were prepared following a modified solvothermal synthesis route. 1-mmol mixed reactant contained $GdCl_3$ ($MgCl_2$), $YbCl_3$, and $ErCl_3$, and the ratio of $GdCl_3$ ($MgCl_2$):$YbCl_3$:$ErCl_3$ was set as 78:20:2. The aforementioned reactants contained with 6 ml of oleic acid (OA) and 15 ml of 1-octadecene (ODE) were added into the 50-ml two-necked flask. At first, in order to form a homogeneous solution they should be heated to 160 °C. Being stirred on the top for 20 min, the solution then was cooled down to room temperature. After that, a mixed solution which contained 10-ml methanol solution, a total of 2.5-mmol NaOH and 4-mmol NH_4F was added. This process must be slowly added into the corresponding flask while stirring drop by drop. The solution which was acquired above was stirred for the determinative 45 min and then heated slowly to 100 °C for 50 min to eliminate the steam of methanol and residual water. Finally, the solution was rapidly heated to 310 °C and then held for another 1.5 hours. All the reactions were under an inert argon atmosphere. After the solution obtained above was completely cooled down to room temperature, they would be centrifuged and washed by cyclohexane and ethanol several times, the final products were dried in a vacuum oven or dispersed in cyclohexane for further characterization.

2.2. Characterization

The x-ray powder diffraction (XRD) was executed utilizing a D/max 2200 V x-ray powder diffractometer with Cu Ka radiation (wavelength = 1.54056 Å). Transmission electron microscopy (TEM) images were taken down on a HEOL-1400F transmission electron microscope operating at an acceleration voltage of 80 kV. High resolution transmission electron microscopy (HR-TEM) images were obtained (FEI Tecnai G^2F20) with an acceleration voltage of 200 kV. With the carbon-coated copper grid as substrates, TEM samples were prepared from a drop of a dilute dispersion of products in cyclohexane dried on the surface of the substrates. UC luminescence spectra were acquired using a SPEX Fluordlog-3 Fluorescence Spectrometer. In addition, the controllable power (BWT Beijing LTD) equipped with a continuous-wave laser (980 nm) was set as an excitation source. In order to ensure the veracity of the comparison among various samples, the emission spectra were tested under the same instrumental parameters. The elements analyses spectra (EDS) were done on a scanning electron microscope (SEM, HITACHI S-4800). The actual chemical compositions were determined by the inductively coupled plasma (ICP) technique utilizing a PerkinElmer Optima 3300DV spectrometer. All the upconversion test methods were implemented at room temperature.

3. Results and discussion

The XRD patterns of the products (Fig. 1) demonstrated the crystallinity and phase transformation of the synthesized nanoparticles with various Mg^{2+} dopant concentrations. All of the synthesized nanoparticles exhibited well-defined peaks, confirming that they were highly crystalline and had sharp diffraction peaks. Then all the diffraction peaks could be indexed to the hexagonal phase of $NaGdF_4$ (JCPDS No. 27-0699) even when the Mg^{2+} doping concentration is as high as 70 mol%. The result indicates the successful synthesis of pure β-$NaGdF_4$ nanocrystals via the amended solvothermal route, which was reflected by the phenomenon that no extra peaks or significant differences were observed. Maybe it is the primary proof that a phase change does not occur after Mg^{2+} ions doping. In addition, as a result of the substitution of Gd^{3+} by the Mg^{2+} ions, the lattice constant and unit-cell

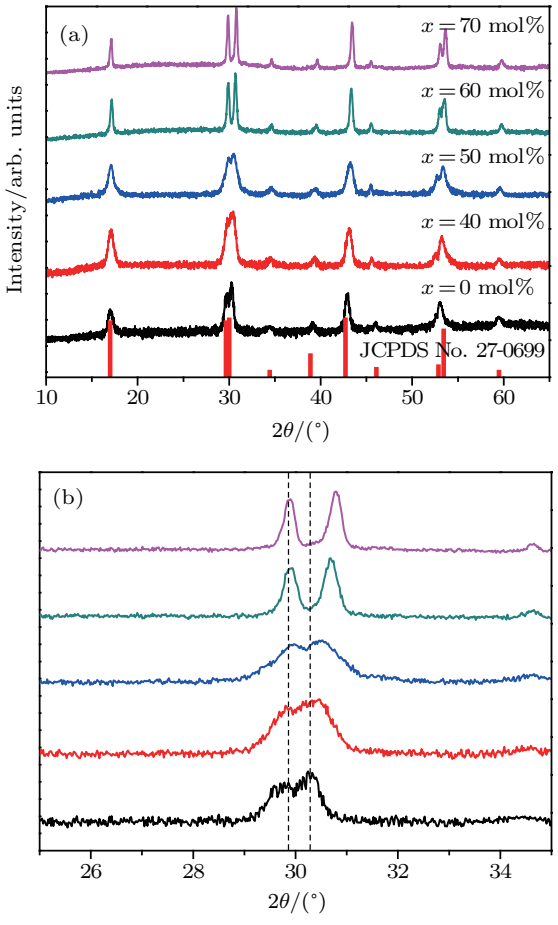


Fig. 1. (color online) (a) XRD patterns of β-$NaGdF_4$:20-mol% Yb^{3+}, 2-mol% Er^{3+}, x mol% Mg^{2+} ($x = 0$, 40, 50, 60, and 70) nanoparticles and (b) amplified XRD patterns of the main diffraction peaks.

volume increased with the increasing Mg^{2+} ion concentration, which caused the diffraction peaks to shift. This shift may have been caused by the alterations in the crystal cell volume following the Mg^{2+} doping. At the same time, the crystallinity of the host has an obvious improvement, which is advantageous for the luminescence of the doped activators.

Parthiban Ramasamy indicated that in the $NaGdF_4$ host lattice, the Fe^{3+} ions appeared via substituting the Gd^{3+} site according to the same charge valence (+3). Then Lei[23] pointed out the results, confirmed the incorporation of Ca^{2+} into $NaGdF_4$ by substituting Gd^{3+}. The charge balance in $NaGdF_4$ is perturbed after Mg^{2+} displacing Gd^{3+}, which should be noted obviously. As shown in previous research work, F^- vacancies were formed in order to maintain the charge balance. A quantitative ICP–MS analysis of the synthesized nanoparticles has further confirmed the formed F^- vacancies (see Table 1). As clearly shown in Table 1, with the increasing of Mg^{2+} doping content, the content of Gd^{3+} decreases correspondingly, and the value of Gd/Mg ratio is the same as the nominal one, whereas the Na content remains unchanged. These situations confirm the incorporation of Mg^{2+} into $NaGdF_4$ by substituting Gd^{3+}. Figure 2 plots SEM images and elements analysis spectra (EDS) of β-$NaGdF_4$:20-mol% Yb^{3+}, 2-mol% Er^{3+} NCs which codoped with 0 mol% to 7-mol% Mg^{2+}. It is notably presented in each element such as Na, Gd, Mg, F, and so on.[24] The result suggested that the peak intensity of Gd^{3+} was reduced while the intensity of Mg^{2+} was increased. All the above results indicate a substitution of Gd^{3+} with Mg^{2+} in $NaGdF_4$ lattice.

Table 1. ICP-MS analysis of the synthesized nanoparticles with different concentrations of Mg^{2+} ions codoping. Sample A: 0 mol% Mg^{2+}; sample B: 40-mol% Mg^{2+}; sample C: 50-mol% Mg^{2+}; sample D: 60-mol% Mg^{2+}; sample E: 70-mol% Mg^{2+}.

Sample	Gd/(Gd+Mg)		Mg/(Gd+Mg)	
	Nominal	Measured	Nominal	Measured
A	0.78	0.78	0	0
B	0.38	0.36	0.40	0.42
C	0.28	0.24	0.50	0.54
D	0.18	0.20	0.60	0.58
E	0.08	0.10	0.70	0.68

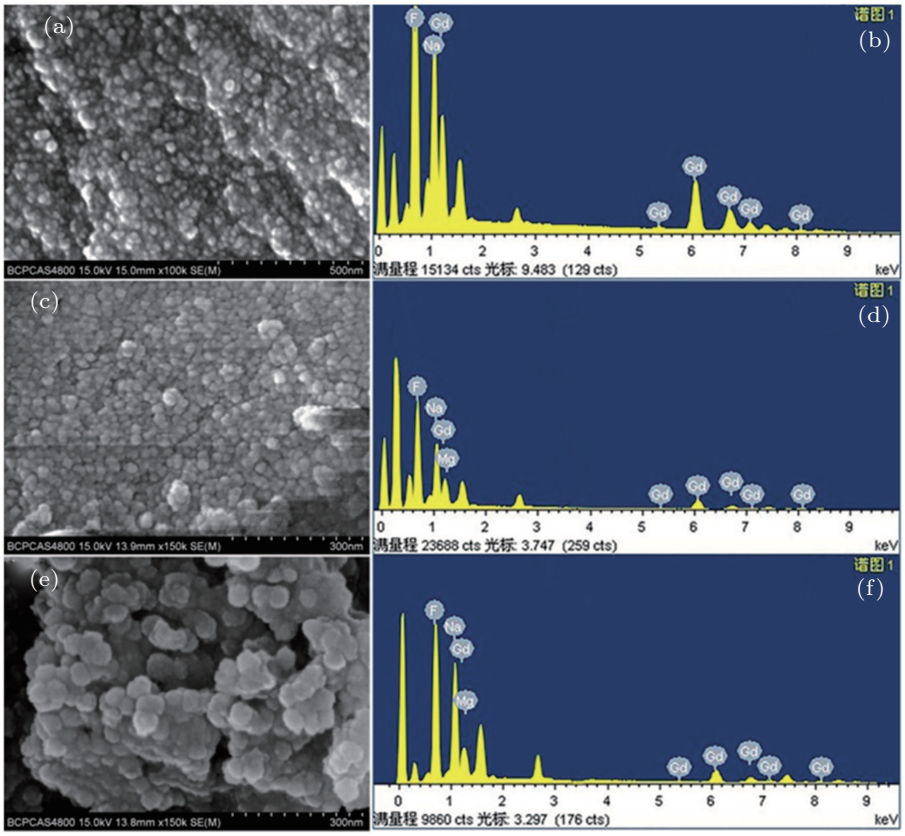


Fig. 2. (color online) SEM images and the EDS spectra of β-$NaGdF_4$:20-mol% Yb^{3+}, 2-mol% Er^{3+} nanoparticles with different Mg^{2+} concentrations (a) and (b): 0 mol%, (c) and (d): 40 mol%, (e) and (f): 60 mol%.

The detailed structures of the β-$NaGdF_4$:20-mol% Yb^{3+}, 2-mol% Er^{3+} nanoparticles were obtained by using TEM and HR-TEM. Figures 3(a)–3(e) show the low-magnification TEM images, which reveals the synthesized hexagonal phase $NaGdF_4$:20-mol% Yb^{3+}, 2-mol% Er^{3+} with the concentrations of 0-mol% to 70-mol% Mg^{2+}. It should be noted that the morphologies of the prepared nanoparticles change obviously. At the same time, figure 3(f) shows the high resolution TEM (HR-TEM) pictures and the SAED pattern of the 60-mol% Mg^{2+}-doped $NaGdF_4$:20-mol% Yb^{3+}, 2-mol% Er^{3+} NCs.

The HR-TEM image shows the high crystalline property of the nanoparticles and the calculated inter-planar distance between the two adjacent lattice planes is 0.52 nm, corresponding to the (100) lattice plane of the hexagonal phase $NaGdF_4$ (JCPDS card No. 27-0699). A perfect hexagonal crystal structure is demonstrated in the corresponding fast Fourier transform (FFT) of the HR-TEM image (inset in panel (f)). The above structure is in good agreement with the XRD result presented in Fig. 1.

The morphology conversion induced by Mg^{2+} doping in $NaGdF_4$:Yb^{3+}, Er^{3+} NCs is shown in Fig. 4(a). As the capping function of excess F^- ions is on the crystal planes, the ratio of F^-/RE^{3+} ions in the reaction solution has a key impact on the morphology of the finally formed $NaREF_4$ NCs. These results have already been confirmed by several research groups.[25–27] The result which had been verified by Wang's group indicated that when the F^-/RE^{3+} ($RE = Gd + Yb + Er$) ratio is set as 4:1 in the present system, no excess F^- is provided. Consistent with the above discussions, in this research when Mg^{2+} is incorporated into the $NaGdF_4$ lattices by substituting Gd^{3+}, F^- vacancies are formed for the sake of maintaining the charge balance. The formation of F^- vacancies results in a conversion of the morphology of Mg^{2+}-doped $NaGdF_4$:Yb^{3+}, Er^{3+} NCs from shaped nanoparticles to hexagonal nanoplates. In order to acquire further proof of the proposed mechanism, two other specimens were synthesized in the same terms and conditions, the morphologies of which were shown in Figs. 4(b)–4(e). 60-mol% Mg^{2+}-doped $NaGdF_4$:20-mol% Yb^{3+}, 2-mol% Er^{3+} NCs with F^- to RE^{3+} ratio of 3.2:1 and $NaGdF_4$:20-mol% Yb^{3+}, 2-mol% Er^{3+} NCs with F^- to RE^{3+} ratio of 4.8:1 were prepared respectively. The morphology is consistent with the result demonstrated from the TEM image of $NaGdF_4$:20-mol% Yb^{3+}, 2-mol% Er^{3+} NCs, and 60-mol% Mg^{2+}-doped $NaGdF_4$:20-mol% Yb^{3+}, 2-mol% Er^{3+} NCs prepared with F^- to RE^{3+} ratio of 4.0:1. It was concluded that the Mg^{2+} doping induced shape evolution in the system originated from excess F^- ions in the solution after the substitution of Gd^{3+} by Mg^{2+}.

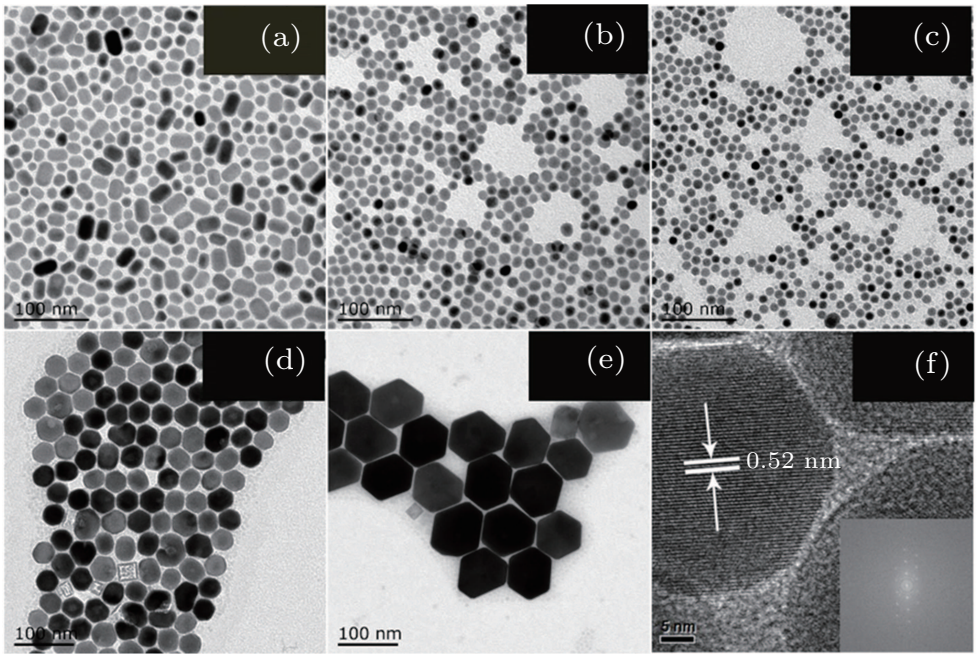


Fig. 3. The TEM images of β-$NaGdF_4$:20-mol% Yb^{3+}, 2-mol% Er^{3+} NCs codoped with (a) 0-mol%, (b) 40-mol%, (c) 50-mol%, (d) 60-mol%, and (e) 70-mol% Mg^{2+} ions; (f) HR-TEM image of a single nanoplate of 60-mol% Mg^{2+} codoped $NaGdF_4$:20-mol% Yb^{3+}, 2-mol% Er^{3+} NCs. Inset: fast Fourier transform (FFT) of the HR-TEM image exhibits a hexagonal symmetry.

Figure 5(a) exhibits the UC emission spectra of β-$NaGdF_4$:20-mol% Yb^{3+}, 2-mol% Er^{3+}, x-mol% Mg^{2+} ($x = 0$, 40, 50, 60, and 70) samples which are dispersed in cyclohexane and excited by a 980-nm cw laser at a power density of 500 $mW{\cdot}cm^{-2}$. The intensity of the UC emission increases gradually with the concentration of codoped Mg^{2+} from 0 mol% to 60 mol%. Then the UC intensity reduces when the concentration of Mg^{2+} is as high as 70 mol% compared to that of the sample of 60 mol%. Obviously, the UC emission intensity of the $NaGdF_4$:20-mol% Yb^{3+}, 2-mol% Er^{3+}:NCs doped with 60-mol% Mg^{2+} reached a maximum in relative terms, which is even higher than the intensity of non-codoped Mg^{2+} in $NaGdF_4$:20-mol% Yb^{3+} 2-mol% Er^{3+} nanoparticles. It is worth mentioned that with the concentration of Mg^{2+} increasing, not only the intensity of green UC emission but also the intensity of red UC emission increase correspondingly. The same trend for the dependence of the red ($^4F_{9/2} \rightarrow {}^4I_{15/2}$) and green ($^2H_{11/2}$, $^4S_{3/2} \rightarrow {}^4I_{15/2}$) emission intensities due to the Mg^{2+} doping (see Fig. 5(b)), which indicates they follow the same UC pathways.

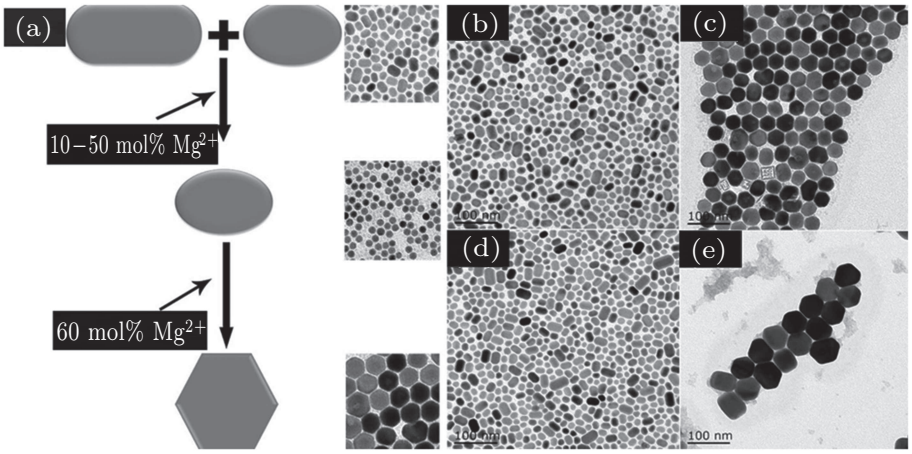


Fig. 4. (a): Schematic illustration of the proposed mechanism for the morphology conversion induced by Mg^{2+} doping in β-$NaGdF_4$: 20-mol% Yb^{3+}, 2-mol% Er^{3+}NCs. (b)–(e): TEM images of (b) $NaGdF_4$: 20-mol% Yb^{3+}, 2-mol% Er^{3+} NCs and (c) 60-mol% Mg^{2+} doped $NaGdF_4$:20-mol% Yb^{3+}, 2 mol% Er^{3+} NCs prepared with F to RE^{3+} ratio of 4.0:1; (d) 60-mol% Mg^{2+}-doped $NaGdF_4$:20-mol% Yb^{3+}, 2-mol% Er^{3+} NCs with F^- to RE^{3+} ratio of 3.2:1; (e) $NaGdF_4$:20-mol% Yb^{3+}, 2-mol% Er^{3+} NCs prepared with F^- to RE^{3+} ratio of 4.8:1 respectively.

To understand the intensity of UC emission for Mg^{2+} codoped β-$NaGdF_4$:20-mol% Yb^{3+}, 2-mol% Er^{3+} nanoparticles in more detail, the main factors affecting UC luminescence of a definite nanophase are considered generally. On the one hand, in view of the crystal structure, β-$NaGdF_4$ is a disordered crystal, the randomly distributed sites of Na^+/Gd^{3+} cations which at the same lattice contribute to multiple active sites for the doping Ln^{3+} ions. With the concentration of Mg^{2+} increasing in the $NaGdF_4$ host, F^- vacancies are generated more and more in order to maintain a charge balance. The amendment of the host crystal structure above all accelerates and diversifies the active sites for the Ln^{3+} ions. Then the number of possible $Yb^{3+} \rightarrow Er^{3+}$ energy-transfer processes increases, attributed to the presence of multiple independent sites for both Yb^{3+} and Er^{3+} ions in the host, which observably increases the probability of an extremely efficient resonant or near-resonant process,[28–30] thus a large enhancement of the UC luminescence for Mg^{2+}-doped samples occurred. On the other hand, depending on the intra 4f transition probability, the UC emissions of Ln^{3+}-doped materials significantly affected by the local crystal field environment of Ln^{3+}. The forbidden 4f–4f transitions of Ln^{3+} is broken efficiently by the intermixing of the f states of Ln^{3+} ions with higher electronic configurations. According to the theory of Judd–Ofelt (J–O),[31] the forbidden transition probability is closely related to the crystal symmetry, and the probability of electric dipole transitions generally can be expressed as

$$W^R(\psi J, \psi' J') = \left[\frac{64\pi^4(\Delta E)^3}{3h(2J+1)}\right] e^2 \frac{1}{9n(n^2+2)^2} \times \sum_{2,4,6} \Omega_t \left|\left\langle \psi J \| U^{(t)} \| \psi' J' \right\rangle\right|^2,$$

where ΔE is energy distance, $|\langle \psi J \| U^{(t)} \| \psi' J' \rangle|$ is the matrix element of transition, Ω_t ($t = 2, 4, 6$) are J–O intensities parameters, which depend on the local environment and symmetry around the Ln^{3+} ions. As to the Ln^{3+}-codoped materials, since the affection from the host property for the forbidden transition probability normally can be neglected, the forbidden transition probability is mainly determined by the local environment and symmetry of the Ln^{3+} ions. Gao *et al.* have used the tervalence Eu^{3+} ions as the probe, which are extremely sensitive to the environment, to study the local environment symmetry of the luminescence center within the $NaYF_4$ and $LiYF_4$ micro-crystals. The result confirms a decrease in the symmetry of the Eu^{3+} ligand field, which is induced by doped ions. The underlying reason for the decrease is that the magnetic $^5D_0 \rightarrow {}^7F_1$ transition does not depend on the the Eu^{3+} ligand field, while the electric dipolar $^5D_0 \rightarrow {}^7F_2$ intensifies with decreasing environmental symmetry. So η can clearly reflect

$$\eta = I_{^5D_0 \rightarrow {}^7F_1} / I_{^5D_0 \rightarrow {}^7F_2},$$

the symmetry of the Ln^{3+} ions, which stated on the local environment. The smaller value of η, the lower the symmetry, and the bigger the transition probability. So the lower crystal symmetry is always beneficial to higher UC intensity. Therefore, F^- vacancies formed (via the substitution of Gd^{3+} by Mg^{2+} ions) in the host should reduce the local crystal field symmetry around Yb^{3+} and Er^{3+} ions. Therefore, the lower symmetry favors the breaking of the forbidden transition of Ln^{3+} and meanwhile it is beneficial to enhancing the UC luminescence. As a result, the intensity of UC emission increases since Mg^{2+} tridoping into the host $NaGdF_4$:20-mol% Yb^{3+}, 2-mol% Er^{3+}.

Moreover, as is well known, a good crystallinity of the host is beneficial for the UC emission of the doped activators.[32] As mentioned above, when the introduced contents of Mg^{2+} ions were increased, the amounts of excess F^- ions in the system were increased significantly, which changes

the reaction environment and subsequently the growth behavior of the $NaGdF_4$:20-mol% Yb^{3+}, 2-mol% Er^{3+} NCs, and results in the modification of their crystallinity.[33,34] With the content of Mg^{2+} ions increasing, the crystallinity of the host has an obvious improvement, corresponding to the XRD patterns (Fig. 1), which is advantageous for the luminescence of the doped activators.

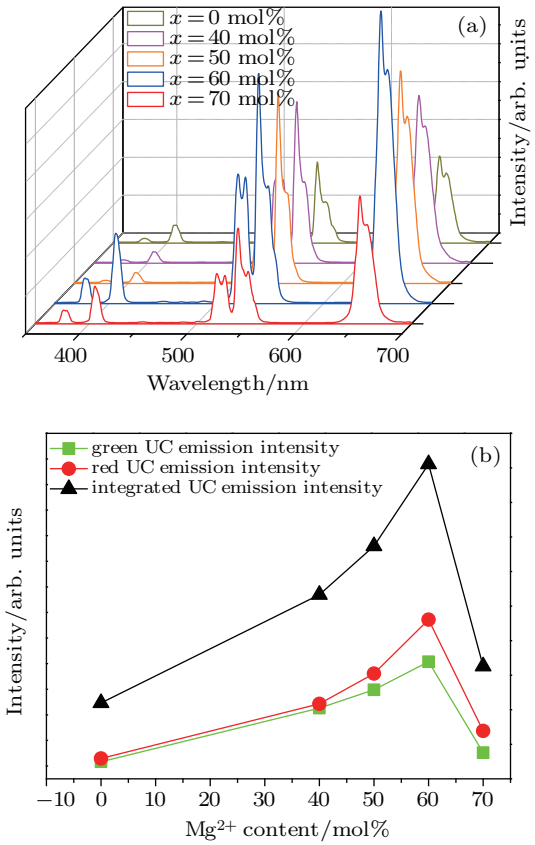


Fig. 5. (color online) (a) UC luminescence spectra of the samples after doping various concentrations of Mg^{2+} ions into the $NaGdF_4$:20-mol% Yb^{3+}, 2-mol% Er^{3+} matrix: x-mol% Mg^{2+} ions under diode laser excitation at 980 nm (x = 0, 40, 50, 60, 70). (b) Red, green, and total UC emission intensities versus Mg^{2+} doping content.

As a function of the pump power for the two samples shown in Figs. 6(a) and 6(b), the luminescence intensities of UC emissions were measured for the sake of measuring the number of photons responsible for the UC mechanism. The dependence of the green and red emissions on the excitation power was calculated according to Auzel's method, $I \propto P^n$, where P is the pumping laser power, and n is the number of laser photons required in populating the upper emitting state.[35] The slope n, which is nearly 2, indicates the following results: 1) both the red and green UC emissions are two photon absorption routes;[36] 2) the Mg^{2+} doping does not affect the UC mechanism.

The diagram of the UC energy-transfer processes demonstrated in Fig. 6(c) explains the emissions. Obviously, they have two successive routes from Yb^{3+}, which could excite Er^{3+} ions to the $^4F_{7/2}$ level, then the Er^{3+} ions relax to the $^2H_{11/2}$ and $^4S_{3/2}$ levels by the non-radiative relaxation processes, followed with the green emission. For the red UC luminescence process, the Er^{3+} ions relax non-radiatively from $^4I_{11/2}$ to the $^4I_{13/2}$ level, and then the $^4I_{13/2}$ level of Er^{3+} ions excited to the $^4F_{9/2}$ level by the Yb^{3+} ion energy transfer. The transition from the $^4F_{9/2}$ level to the ground state yields the red UC emission.

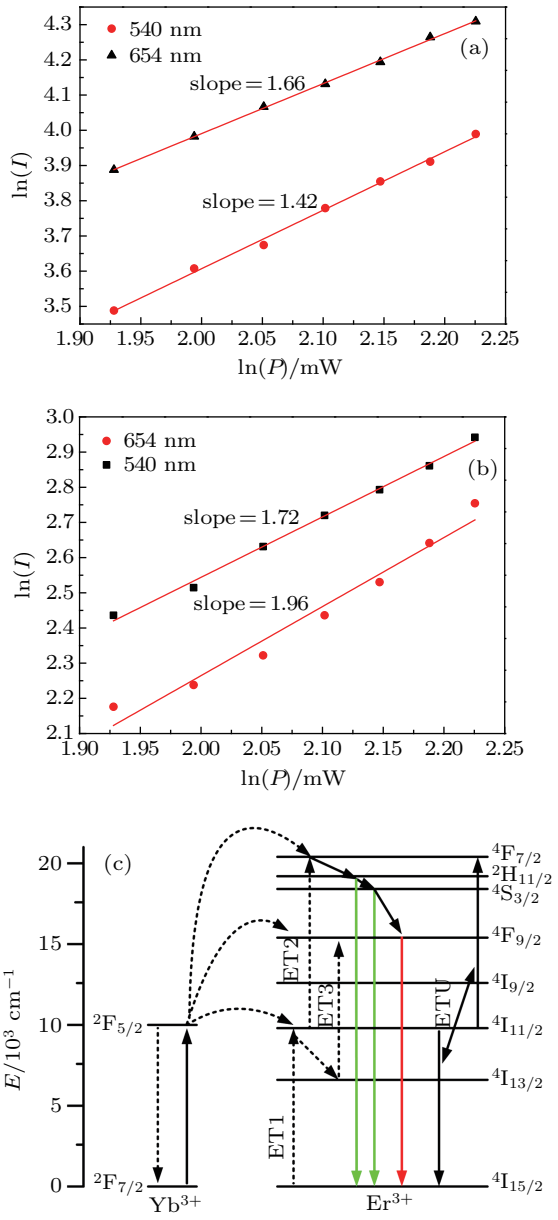


Fig. 6. (color online) (a) and (b): Power dependence of UC emissions of $NaGdF_4$:20-mol% Yb^{3+}, 2-mol% Er^{3+} of (a) 0-mol% and (b) 6-mol% Mg^{2+} dispersions in cyclohexane with a 980-nm semiconductor laser. (c): Energy level diagrams of Er^{3+} and Yb^{3+} ions, showing possible energy transfer mechanisms for red and green UC emissions of Er^{3+} activators in the hosts.

4. Conclusions

In summary, β-$NaGdF_4$ codoped with 20-mol% Yb^{3+}, 2-mol% Er^{3+} and 0-, 40-, 50-, 60-, and 7-mol% Mg^{2+} were synthesized. We demonstrated that with the concentration of Mg^{2+} increasing, the morphology of the nanoparticles turns to

change gradually and the UC emission is increased gradually as well. When doped with 60-mol% Mg^{2+}, the UC emission intensity of nanoparticles reached the maximum level. The effect of Mg^{2+}: 1) lowering the local crystal field symmetry around the Ln^{3+} activators, 2) improving the crystallinity of the $NaGdF_4$ NCs. With increasing Mg^{2+} doping content, the above two factors all induce a gradual intensification in the UC luminescence. As a consequence, the 60-mol% Mg^{2+}-doped samples exhibit the best UC performance. This work significantly codoped Mg^{2+} into β-$NaGdF_4$:20-mol% Yb^{3+}, 2-mol% Er^{3+} NCs, which has a great potential in some fields such as photocatalysis, biomedicine, and solar cells.

References

[1] Wang F, Han Y, Lim C S, Lu Y H, Wang J, Xu J, Chen H Y, Zhang C, Hong M H and Liu X G 2010 *Nature* **463** 1061

[2] Gao W, Dong J, Wang R B, Wang Z J and Zheng H R 2016 *Acta Phys. Sin.* **65** 084205 (in Chinese)

[3] Zhao C, Meng Q Y and Sun W J 2015 *Acta Phys. Sin.* **64** 107803 (in Chinese)

[4] Dai L, Liu C R, Tan C, Yan Z H and Xu Y H 2017 *Chin. Phys. B* **26** 044207

[5] Du X Y, Wang X F, Meng L, Bu Y Y and Yan X H 2017 *Nanoscale Res. Lett.* **12** 163

[6] Dai G T, Zhong Z Q, Wu X F, Zhan S P, Hu S G, Hu P, Hu J S, Wu S B, Han J B and Liu Y X 2017 *Nanotechnology* **28** 155702

[7] Dong B, Xu S, Sun J, Bi S, Li D, Bai X, Wang Y, Wang L P and Song H W 2011 *J. Mater. Chem.* **21** 6193

[8] Wang F, Banerjee D, Liu Y S, Chen X Y and Liu X Q 2010 *Analyst.* **135** 1839

[9] Ding M Y, Chen D Q, Wan Z Y, Zhou Y, Zhong J S, Xi J H and Ji Z Q 2015 *J. Mater. Chem. C* **3** 5372

[10] Liu J, Chen G Y, Hao S W and Yang C H 2017 *Nanoscale* **9** 91.

[11] Biju S, Harris M, Vander Elst L, Wolberg M, Kinschhock C and Parac-Vogt T N 2016 *Rsc. Adv.* **6** 61443

[12] Wu S J, Duan N, Shi Z, Fang C C and Wang Z P 2014 *Anal. Chem.* **86** 3100

[13] Wang Y H, Wang H G, Liu D P, Song S Y, Wang X and Zhang H J 2013 *Biomaterials* **34** 7715

[14] Huang X Y 2016 *Dyes Pigments* **130** 99

[15] Shan G B and Demopoulos G P 2010 *Adv. Mater.* **22** 4373

[16] Huang X Y, Han S Y, HuangW and Liu X Q 2013 *Chem. Soc. Rev.* **42** 173

[17] Krämer K W, Biner D, Frei G, Güdel H U, Hehlen M P and Lüthi S R 2004 *Chem. Mater.* **16** 1244

[18] Aebischer A, Hostettler M, Hauser J, Krämer K, Weber T, Güdel H U and Bürgi H B 2006 *Angew. Chem.* **118** 2869

[19] Yi J, Qu J B, Wang Y A and Zhou D C 2014 *Chin. Phys. B* **23** 104224

[20] Yang J Z, Qiu J B, Yang Z W, Song Z G, Yang Y and Zhou D C 2015 *Acta Phys. Sin.* **64** 138101 (in Chinese)

[21] Li D, Ma Q L, Xi X, Dong X T, Yu W S, Wang J X and Liu G X 2017 *Chem. Eng. J.* **309** 230

[22] Ramasamy P, Chandra P, Rhee S W and Kim J 2013 *Nanoscale* **5** 8711.

[23] Lei L, Chen D Q, Xu J, Zhang R and Wang Y S 2014 *Chem. Asian J.* **9** 728

[24] Gao W, Zheng H R, Han Q Y, He E J, Gao F Q and Wang R B 2014 *J. Mater. Chem. C* **2** 5327

[25] Wang L Y and Li Y D 2007 *Chem. Mater.* **19** 727

[26] Liang X, Wang X, Zhuang J, Peng Q and Li Y 2007 *Adv. Funct. Mater.* **17** 2757

[27] Zeng S J, Ren G Z, Xu C F and Yang Q B 2011 *CrystEngComm.* **13** 1384.

[28] Krämer K W, Biner D, Frei G, Güdel H U, Hehlen M P and Lüthi S R 2004 *Chem. Mater.* **16** 1244

[29] Aebischer A, Hostettler M, Hauser J, Krämer K, Weber T, Güdel H U and Bürgi H B 2006 *Angew. Chem.* **118** 2869

[30] Blasse G and Grabmaier B C 1994 *Luminescent Materials* (Berlin/Heidelberg: Springer) p. 91

[31] Judd B R 1962 *Phys. Rev.* **127** 750

[32] Zhao C Z, Kong X G, Liu X M, Tu L P, Wu F, Zhang Y L, Liu K, Zeng Q H and Zhang H 2013 *Nanoscal* **5** 8084

[33] Wang L Y and Li Y D 2007 *Chem. Mater.* **19** 727

[34] Zeng S J, Ren G Z, Xu C F and Yang Q B 2011 *CrystEngComm.* **13** 1384

[35] Di Q M, Sun Y M, Xu Q G, Han L, Xue B and Sun J Y 2015 *Chin. Phys. B* **24** 067801

[36] Dai L, Xu C, Zhang Y, Li D Y and Xu Y H 2013 *Chin. Phys. B* **22** 094201